Pergamon

Int. J. Heat Mass Transfer. Vol. 40, No. 15, pp. 3503–3511, 1997

Printed in Great Britain
0017–9310/97 $17.00+0.00

PII: S0017-9310(97)00017-3

Using the finite element method to compute the influence of complex porosity and inclusion structures on the thermal and electrical conductivity

K. BAKKER

Netherlands Energy Research Foundation ECN, P.O. Box 1, 1755 ZG Petten, The Netherlands

(*Received* 7 *September* 1995 *and in final form* 9 *January* 1997)

Abstract—The finite element method (FEM) is used to compute the conductivity of a matrix that contains a dispersed phase, which can be porosity or inclusions. The FEM accounts for the influence of shape, orientation and distribution of the dispersed phase on the conductivity. From these computations the two dimensional conductivity is obtained, that represents a useful lower limit of the real conductivity which is three dimensional. A relation has been derived that transfers the two dimensional conductivity into the real conductivity. As an example the influence of the microstructure of irradiated UO_2 on the conductivity is calculated. © 1997 Elsevier Science Ltd.

1. INTRODUCTION

Porosity and inclusions change the thermal and the electrical conductivity of many materials. Various equations, both empirical and analytical, have been developed to describe this influence. A large spread exists between the results of various empirical formulas [1–3]. This spread is likely due to a large diversity in the shape and the orientation of the porosity and inclusions in various materials, which can not be accounted for in the equations. Several analytical equations describe the influence of porosity and inclusions on the conductivity [4–10]. In a recent paper [11] these analytical equations were compared with results from the finite element method (FEM), and it was concluded that the analytical equation of Schulz [6] gives the best representation of the influence of a dispersed phase on the overall conductivity. However, the equation of Schulz [6] can only give a good approximation of the overall thermal conductivity when the pores and inclusions have an ellipsoidal shape and are randomly positioned with respect to each other. When the equation of Schulz is used to compute the conductivity of materials that do not fulfil the above mentioned properties a considerable inaccuracy will be induced.

For many materials, e.g. UO_2 pellets that have been irradiated in a nuclear reactor, the structure of the porosity or inclusions is complex (Fig. 1). In these UO_2 pellets the pores tend to collect at the grain boundaries and cannot be characterized by ellipsoids and, as a consequence, cannot be accurately described by the equation of Schulz [6]. In this paper the FEM is used to compute the conductivity of complex porosity or inclusion structures. The FEM accounts for the influence on the conductivity of the shape, the orientation and the distribution of the porosity and the inclusions in a more accurate way than by trying to apply the analytical equations of Schulz to these complex pore shapes.

2. FINITE ELEMENT METHOD COMPUTATIONS

A photograph of a cross-section of a material containing a dispersed phase yields only a two-dimensional (2D) image of the three-dimensional (3D) microstructure. It is impossible to fully reconstruct the exact 3D shape of the microstructure from the 2D photograph. Furthermore, it is impossible to make 3D finite element method (FEM) conductivity calculations on a complex 3D microstructure, due to the limited capacity of computers. For these reasons FEM conductivity computations have been performed using a 2D photograph, which yields the conductivity in the plane of the photograph (called 2D conductivity). A relation that transfers the 2D conductivity into the real (3D) conductivity is discussed in Section 3.

A photograph of a cross section of a piece of material has been made in such a way that the thermal gradient is positioned in the plane of the photograph (Fig. 1). The 2D thermal conductivity of the microstructure marked in Fig. 1 has been computed as an example of the use of the FEM. This geometry has been entered in the commercially available FEM program Ansys, that describes the microstructure with triangular elements. In this example the thermal conductivity of the UO_2 matrix was arbitrarily assumed to be ten times larger than that of the gas in the pores. The left and the right boundary of the area used for

NOMENCLATURE

a_{iD}	constants that characterize the influence of the shape of the dispersed phase particles on the i ($i = 2, 3$) dimensional conductivity
c_D	concentration of dispersed phase material
f_{iD}	i dimensional ($i = 2, 3$) conductivity of the material containing the dispersed phase divided by the conductivity of the fully dense material
l_i	length of the ellipsoids in the i-direction ($i = x, y, z$)
n	form factor
r	a_{2D}/a_{3D}, that is a function of λ_D/λ_M
T_1	arbitrary temperature
T_2	arbitrary temperature.

Greek symbols

λ_C	conductivity of the mixed material
λ_D	conductivity of the dispersed phase
λ_M	conductivity of the matrix phase.

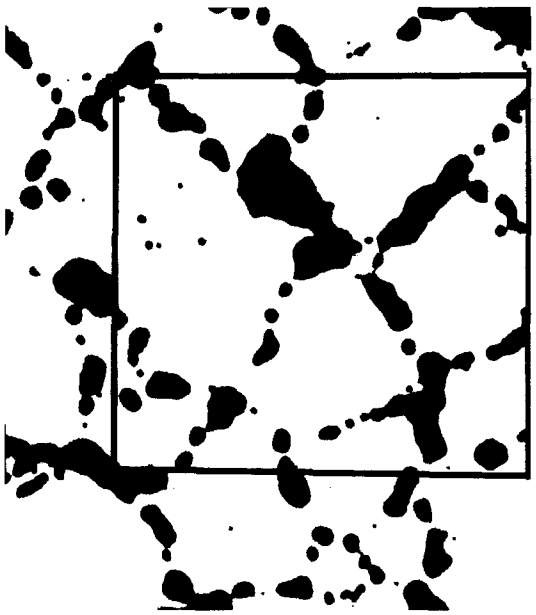

Fig. 1. A part of the cross-section of a UO_2 pellet. The light area is the UO_2 matrix, the dark areas are pores. The marked region has been used for the FEM calculations.

the FEM computation are taken adiabatic. The lower and the upper boundary of this area have the arbitrary temperatures T_1 and T_2, respectively. Consequently, the thermal gradient points in the y-direction. From these calculations the 2D temperature distribution (Fig. 2) and the distribution of the y-component of 2D thermal flux (Fig. 3) were obtained for this pore structure.

The FEM program computes the 2D thermal conductivity from the 2D thermal-flux profile. The 2D conductivity of Fig. 1 amounts to 69% of the conductivity of the fully dense material. The concentration of dispersed phase material (c_D) is also determined during the FEM computations, for the geometry in Fig. 1 c_D equals 0.167. In the absence of corrections the 2D conductivity results yield only a rough estimation of the 3D conductivity. Using equation (1), that will be discussed in Section 3 and the 2D conductivity that amounts to 69%, it is calculated that the 3D conductivity of the microstructure shown in Fig. 1 amounts approximately to 76% of the conductivity of the fully dense material. This result is more accurate than the results that can be obtained by applying an analytical equation to this problem.

The extra degree-of-freedom of the flux in the 3D case compared to the 2D case, causes the 3D conductivity to be larger than the 2D conductivity, irrespective whether the conductivity of the dispersed phase is larger or smaller than that of the matrix material. Hence, the 2D conductivity can be considered as a lower limit of the 3D conductivity.

3. THE 2D AND THE 3D CONDUCTIVITY

3.1. *General relation*

In the previous section it has been discussed that analysing the 2D microstructure yields only a lower limit of the 3D conductivity. However, a 3D microstructure with such a shape that it influences the 3D conductivity strongly, has 2D cross-sections that influence the 2D conductivity strongly. Hence, a relation exists between the computed 2D conductivity and the actual 3D conductivity. This makes it possible to determine the 3D thermal conductivity from the 2D conductivity, without specific knowledge of the 3D shape of the dispersed phase. Hereafter an example will be given that demonstrates the above mentioned relation.

In 3D material that contains only (3D) spherical pores a photograph of this material will be completely different from a photograph of a 3D material that contains only (3D) randomly ordered disk shaped pores. The photograph of the material with spherical pores shows only circular cross sections, while the photograph of the material with the disk shaped pores shows nearly only rectangular cross-sections. Only in the rare case that one of the disks is oriented exactly parallel to the plane of the photograph a circular

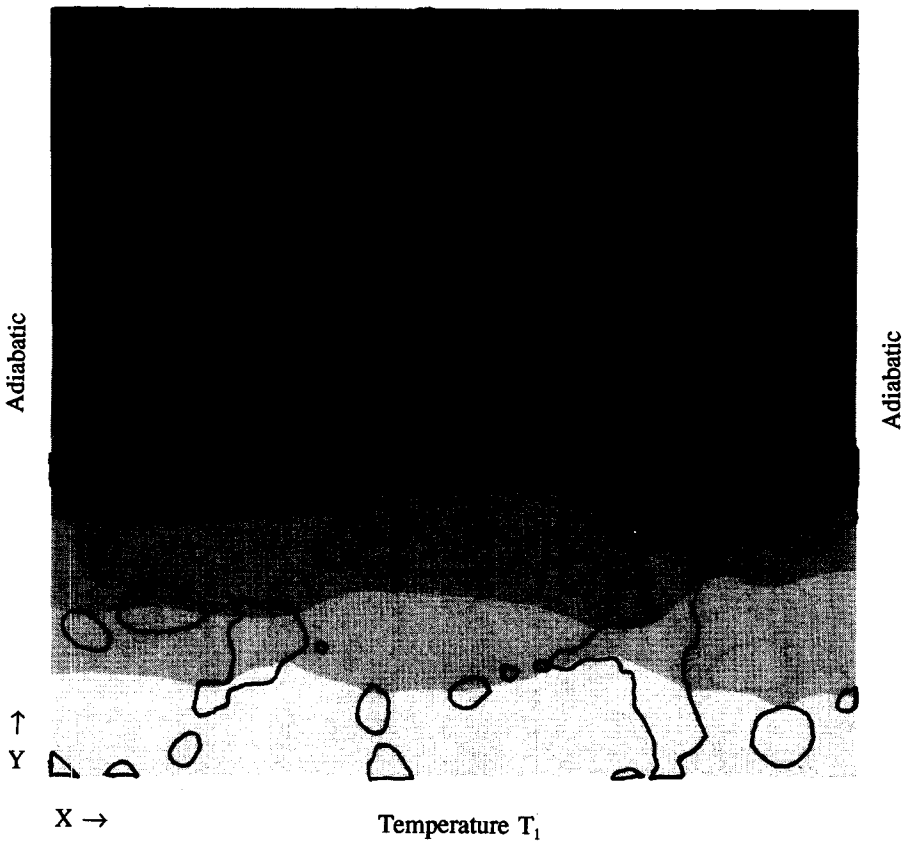

Fig. 2. The 2D temperature distribution as obtained from FEM computations on the microstructure marked in Fig. 1. The lines mark the boundaries of the pores.

cross-section will be seen on the photograph. A photograph of this porous material will, consequently, show a large amount of rectangles and few circular pores. It can be concluded that a non-trivial relation exists between the 3D and the 2D shape. When the 3D disk shaped randomly ordered pores are non-conducting, they will have a much stronger influence on the 3D thermal conductivity than 3D spherical non-conducting pores for the same amount of porosity. 2D rectangular, randomly ordered, pores will have a much stronger influence on the 2D thermal conductivity than 2D spherical pores for the same amount of porosity. Consequently, for 3D pore shapes that cause the 3D thermal conductivity to be low the 2D thermal conductivity is also low. Hence, a physically meaningful relation exists between the 2D and the 3D thermal conductivity.

The relation between the 2D and the 3D conductivity is obtained by analyzing materials that contain pores or inclusions with a simple shape. Simple shapes are used since their influence on the thermal conductivity can be analysed exactly, both in 2D and in 3D, using the analytical equation of Schulz [6]. Such calculations have been performed for two different shapes of the dispersed phase: circular/spherical (Section 3.2) and elliptical/ellipsoidal (Section 3.3). A relation between the concentration of dispersed phase material, the 2D and the 3D conductivity has been obtained (equations (1) and (2)), that depends on the ratio of the conductivity of the matrix and that of the dispersed phase and that is nearly independent of the shape of the dispersed phase. This relation can be used for the complex dispersed phase shapes described with the FEM, which makes it possible to determine the 3D conductivity from the FEM computed 2D conductivity.

$$\frac{1-((1-(\lambda_D/\lambda_M))c_D)-f_{2D}}{1-((1-(\lambda_D/\lambda_M))c_D)-f_{3D}} = r \quad (\lambda_D < \lambda_M) \quad (1)$$

$$\frac{f_{3D}-b}{f_{2D}-b} = \frac{1}{r} \quad (\lambda_D > \lambda_M) \quad (2)$$

where

$$b = \frac{\lambda_D \lambda_M}{c_D \lambda_M + \lambda_D - (c_D \lambda_D)}$$

c_D is the concentration of dispersed phase material, f_{2D} and f_{3D} are the conductivities of the material containing the dispersed phase, in the 2D and the 3D case, respectively, divided by the conductivity of the fully dense material. λ_D and λ_M are the conductivity of the dispersed phase and the matrix phase, respectively. r is a parameter that depends on λ_D/λ_M. In the next two sections the value of r is calculated for various shapes of the dispersed phase particles, various

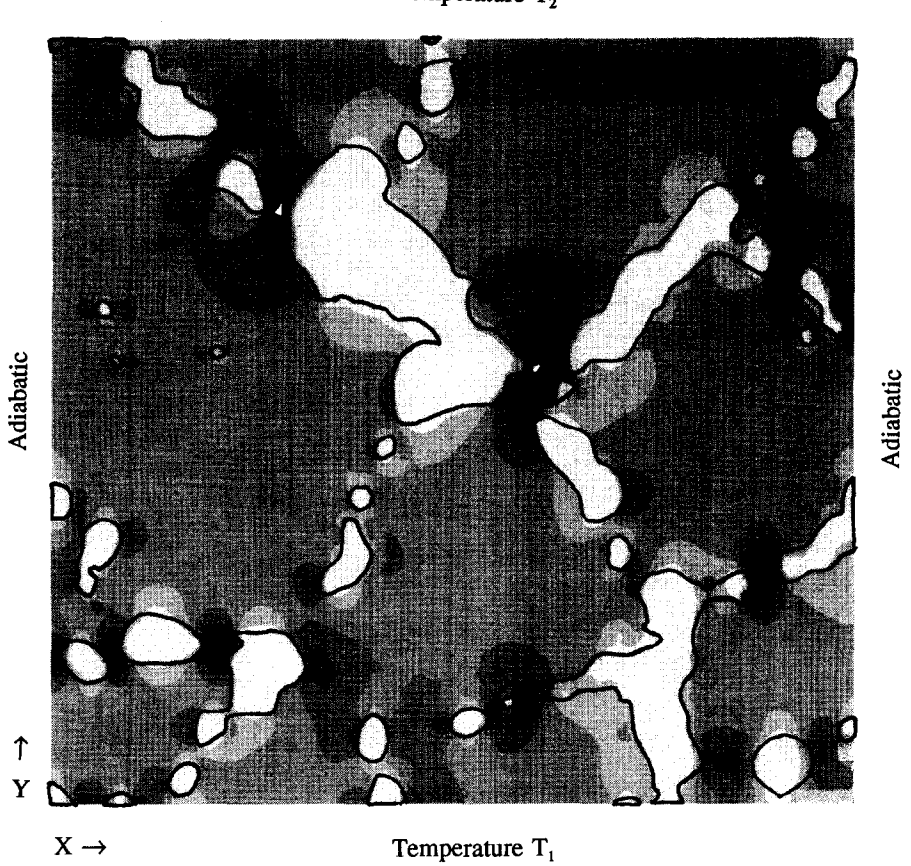

Fig. 3. The 2D distribution of the y-component of the thermal flux, as obtained from FEM computations on the microstructure marked in Fig. 1. The dark regions represent a larger flux than the light regions. The lines mark the boundaries of the pores.

values of c_D and for various values of λ_D/λ_M. It is concluded in Section 3.4 that r depends on λ_D/λ_M and that r hardly depends on the amount of dispersed phase material and on the shape of the dispersed phase particles. The derivation of the equations (1) and (2) is discussed in detail in the Appendix.

The equations (1) and (2) are only valid when the dispersed phase has no preferential orientation in the plane perpendicular to the gradient. Such preferential orientation causes the shape of the cross-sections of the dispersed phase on a photograph to vary considerably, depending on the angle between the photograph and the preferential orientation. This variation makes the transfer of the 2D conductivity into the 3D conductivity, as performed by equations (1) and (2), impossible. A preferential orientation of the dispersed phase in the direction of the gradient can be accepted. Such a preferential orientation does not induce an angular variation in the shape of the cross-sections of the dispersed phase, due to the constant orientation of the photograph with respect to the direction of the preferential orientation of the dispersed phase. The restrictions on the preferential orientation are made under the assumption that the conductivity is determined in the direction of the gradient.

3.2. *Circular (2D) and spherical (3D) particles*

The cross-section of a spherical particle is always a circular particle. This simple relation between the shape of the particle and the shape of the cross-section eases the calculation of r drastically. In this section a comparison is made of the conductivity of a matrix containing circular (2D) or spherical (3D) particles as a dispersed phase. The equations (3) and (4) were derived analytically by Schulz [6] and take the interactions between the dispersed phase material into account. For randomly ordered circular (2D) porosity or inclusions holds:

$$1-c_D=\frac{\lambda_D-\lambda_C}{\lambda_D-\lambda_M}\left(\frac{\lambda_M}{\lambda_C}\right)^{1/2} \tag{3}$$

where λ_C is the conductivity of the mixed material ($\lambda_C=f_{2D}\lambda_M$). For randomly ordered spherical (3D) porosity or inclusions holds:

$$1-c_D=\frac{\lambda_D-\lambda_C}{\lambda_D-\lambda_M}\left(\frac{\lambda_M}{\lambda_C}\right)^{1/3} \tag{4}$$

where λ_C equals $f_{3D}\lambda_M$. For $\lambda_D<\lambda_M$ the values of r, that were calculated for $c_D=0.1$ and 0.2 using the equations (1)–(4), are shown in Fig. 4. For $\lambda_D>\lambda_M$

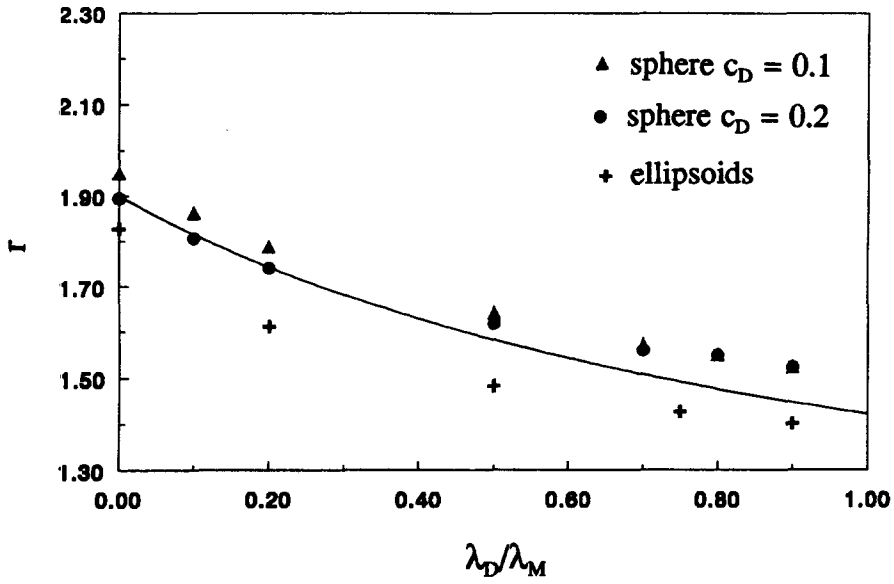

Fig. 4. The dependence of r on λ_D/λ_M ($\lambda_D < \lambda_M$) for ellipsoidal inclusions (+) and spherical inclusions for $c_D = 0.1$ (▲) and 0.2 (●). The line is described by equation (7).

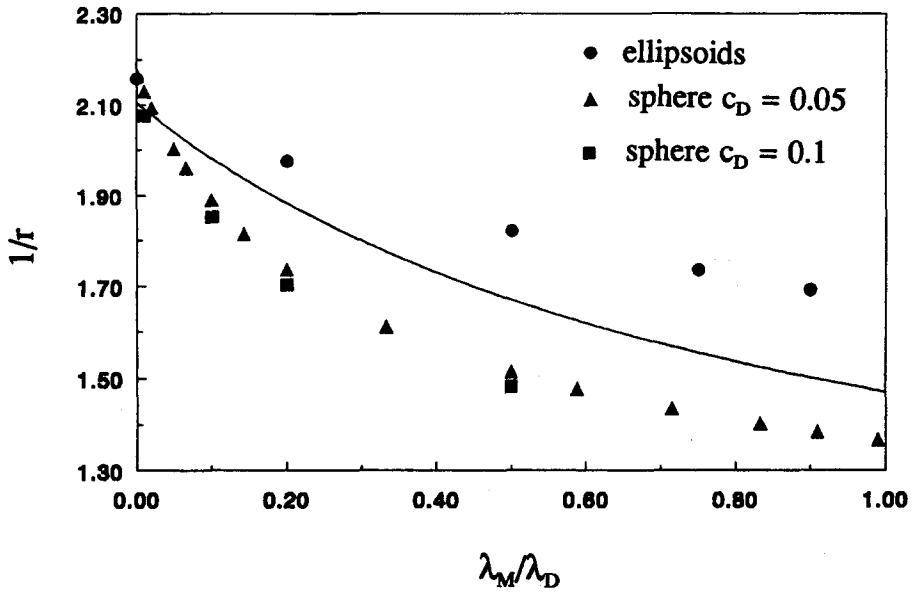

Fig. 5. The dependence of $1/r$ on λ_M/λ_D ($\lambda_D > \lambda_M$) for ellipsoidal inclusions (●) and spherical inclusions for $c_D = 0.05$ (▲) and 0.1 (■). The line is described by equation (8).

the values of $1/r$ were calculated for $c_D = 0.05$ and 0.1 using the equations (1)–(4) and are shown in Fig. 5. These results are discussed in Section 3.4.

3.3. *Elliptical (2D) and ellipsoidal (3D) particles*

In this section a comparison is made with equation (5) [4, 6, 12] of the conductivity of a matrix containing particles with an elliptical (2D) or an ellipsoidal (3D) shape. This equation describes a 3D matrix with ellipsoidal particles. The interactions between the particles are neglected and the rotational axis of the ellipsoids is chosen to be parallel to the gradient. Equation (5) can also describe a 2D matrix with 2D elliptical pores or inclusions by choosing the length of one of the axes, that are oriented perpendicular to the gradient, infinitely long.

$$f_{iD} = 1 + c_D\left(\frac{\lambda_D - \lambda_M}{\lambda_M + (\lambda_D - \lambda_M)n}\right) \quad (i = 2, 3) \qquad (5)$$

The form factor n ($n > 0$), that can be derived both for a 2D and a 3D configuration, depends on the shape of the ellipsoids:

$$n = \frac{1}{2} l_x l_y l_z \int_0^\infty \frac{ds}{(s + l_x^2)\sqrt{(s + l_x^2)(s + l_y^2)(s + l_z^2)}} \qquad (6)$$

Table 1. f_{2D} and f_{3D} of a matrix containing elliptical/ellipsoidal particles with $c_D = 0.05$ and $\lambda_D/\lambda_M = 0.5$

Ratio	f_{2D}	f_{3D}
0.250	0.97222	0.97402
0.333	0.97143	0.97356
0.400	0.97034	0.97319
0.500	0.97000	0.97262
0.666	0.96875	0.97170
1.000	0.96667	0.97000
1.500	0.96429	0.96783
2.000	0.96250	0.96605
2.500	0.96112	0.96458
3.000	0.96000	0.96336
4.000	0.95833	0.96143
Average	0.96601	0.96894

l_x, l_y and l_z are the length of the ellipsoids in the x-, y- and z-direction, respectively. The gradient is directed in the x-direction. s is the integration variable. The integrations have been performed numerically.

In this section both 2D and 3D conductivity calculations were performed with equation (5). In the 3D case the lengths of both axes perpendicular to the gradient were chosen equal ($l_y = l_z$). When this ellipsoid is cut by a plane with the vector of the gradient in it, the cross-section has a constant shape, independent of the cutting plane. This cross-section is an ellipse with the same ratio of the length of the rotation axis and the other axis as that of the ellipsoid. The position of the cutting plane influences the size of the cross-section, but it does not influence the shape of the cross-section. The simple relation between the shape of the 3D ellipsoid and the shape of the 2D cross-section facilitates the calculation of r drastically. Table 1 shows the results of 2D and 3D conductivity calculations, that were performed for $c_D = 0.05$ and $\lambda_D/\lambda_M = 0.5$ for various ellipsoids. Ratio is the length of the axis parallel to the gradient divided by the length of the axis perpendicular to the gradient. Ratio is equal for the 2D and the 3D calculations. Since the interactions between the pores or inclusions are not taken into account in equation (5), a linear relation between c_D and both f_{2D} and f_{3D} exists which causes r to be independent of c_D.

The average values in the last row of Table 1 are obtained by averaging over the ratio values shown in Table 1. The average values of both f_{2D} and f_{3D} are used to calculate, using equation (1) or (2), an effective r value for a particular λ_D/λ_M-value. This procedure has been repeated for a large range of λ_D/λ_M-values, both for $\lambda_D < \lambda_M$ and for $\lambda_D > \lambda_M$. The thus-obtained r-values are included in Figs 5 or 6 and are discussed in Section 3.4.

3.4. *The relation between* r *and* λ_D/λ_M

The values of r obtained in the previous two sections are shown in Fig. 4 ($\lambda_D < \lambda_M$) and Fig. 5 ($\lambda_D > \lambda_M$). The data in Fig. 4 have been fitted to the empirical relation:

$$r = 0.93 + \frac{1}{(\lambda_D/\lambda_M) + 1.03} \quad (\lambda_D < \lambda_M). \tag{7}$$

The data in Fig. 5 have been fitted to the empirical relation:

$$\frac{1}{r} = 0.93 + \frac{1}{(\lambda_M/\lambda_D) + 0.85)} \quad (\lambda_M < \lambda_D). \tag{8}$$

The data in Fig. 5 have been plotted as l/r instead of as r, in order to show the similarity of equations (7) and (8). The variation in $r(\lambda_D < \lambda_M)$ or $l/r(\lambda_D > \lambda_M)$ for various pore or inclusion shapes is approximately 0.3, which yields an error in f_{3D} that is small compared to the error in f_{3D} when it is obtained using an analytical equation. The use of equations (1) or (2) combined with equations (7) or (8) makes it possible to transfer f_{2D}, as obtained from the FEM, into f_{3D}.

4. RESULTS

As an example of the use of the FEM f_{2D} of the microstructure shown in Fig. 1 has been computed for various values of λ_D, while λ_M is 1.0. These f_{2D} values have been converted into f_{3D} values using the equations (1), (2), (7) and (8). The thermal conductivity of a matrix containing spherical particles (equation (4)) has also been calculated for various λ_D values. The f_{2D}, f_{3D} and spherical inclusion values are shown in Fig. 6 for $\lambda_D < \lambda_M$ and in Fig. 7 for $\lambda_D > \lambda_M$.

The influence of the dispersed phase ($\lambda_D < \lambda_M$) on the overall conductivity, as described by f_{2D}, f_{3D} and equation (4) (Fig. 6), has a comparable shape, but the magnitude of the effect differs. f_{2D} can be determined accurately and represents a lower limit of the thermal conductivity (both for $\lambda_D < \lambda_M$ and for $\lambda_D > \lambda_M$), which makes the 2D conductivity an important parameter. In the case of randomly ordered inclusions with $\lambda_D < \lambda_M$, the upper limit of the thermal conductivity is described by the thermal conductivity of spherical inclusions (equation (4)). The difference between the lower and the upper limit is relatively small, which shows the importance of both f_{2D} and equation (4).

The influence of the dispersed phase ($\lambda_D > \lambda_M$) on the overall conductivity, as described by f_{2D}, f_{3D} and equation (4) (Fig. 7), has a comparable shape, but the magnitude of the effect differs. The overall conductivity saturates for large λ_D-values. The conductivities for $\lambda_D = 100\,000$ (not shown) are only slightly larger than those for $\lambda_D = 100$. In the case of randomly ordered inclusions with $\lambda_D > \lambda_M$ the thermal conductivity of spherical inclusions (equation (4)) represents a lower limit of f_{3D}. Hence, for $\lambda_D > \lambda_M$ both spherical inclusions and f_{2D} represent a lower limit of f_{3D}. Figure 7 shows that the difference between both lower limits is rather small for the microstructure of Fig. 1. For microstructures containing strongly elongated inclusions the f_{2D} value is larger than the value obtained from spherical inclusions, while for a microstructure containing relatively spherical

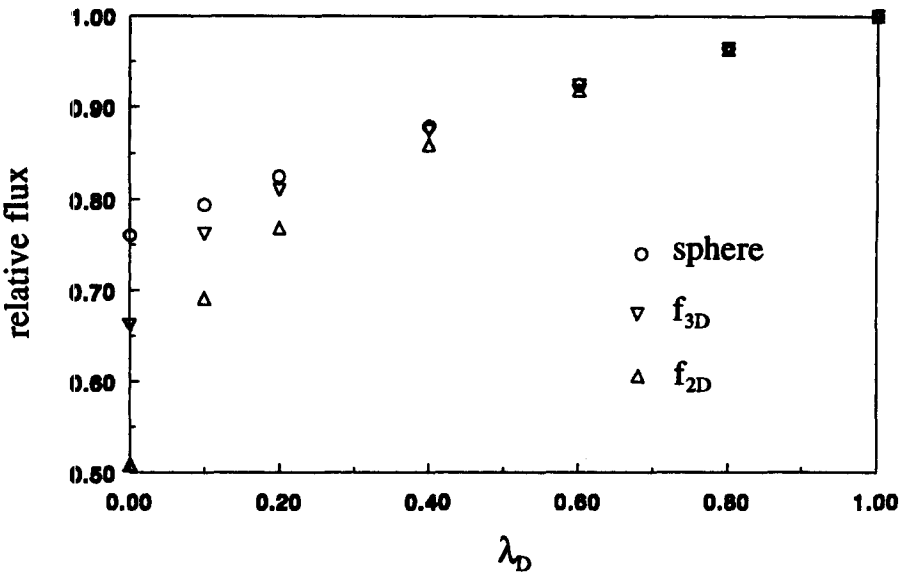

Fig. 6. The values of f_{2D} and f_{3D} for the microstructure marked in Fig. 1 and the thermal conductivity of a matrix containing spherical particles (equation (4)) for $\lambda_D < 1$ ($\lambda_M = 1$).

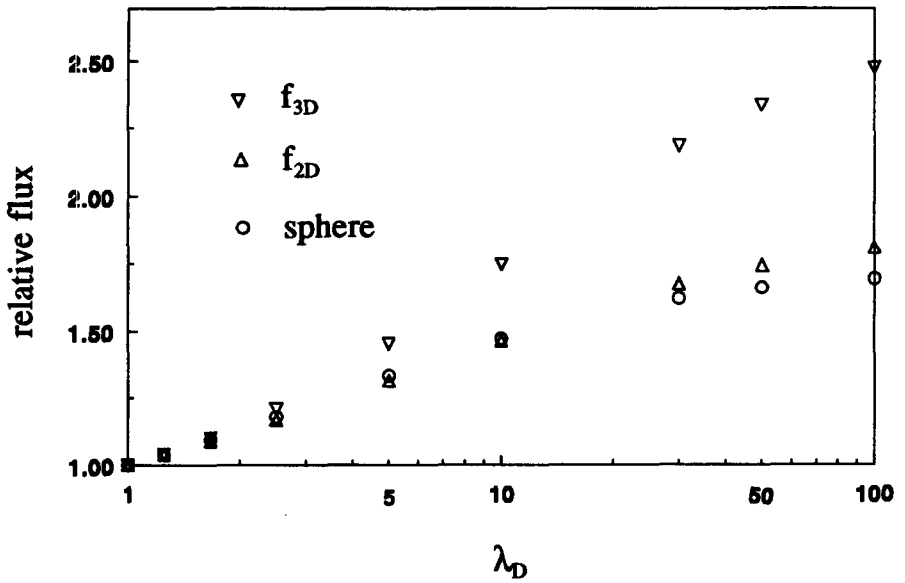

Fig. 7. The values of f_{2D} and f_{3D} for the microstructure marked in Fig. 1 and the thermal conductivity of a matrix containing spherical particles (equation (4)) for $\lambda_D > 1$ ($\lambda_M = 1$).

inclusions the value obtained from equation (4) will be larger than f_{2D}. Hence, for $\lambda_D > \lambda_M$ the lower limit of the thermal conductivity closest to f_{3D} is given by equation (4) for a microstructure with relatively spherical inclusions, while for a microstructure with elongated inclusions f_{2D} yields the most useful lower limit. An upper limit of the thermal conductivity for $\lambda_D > \lambda_M$ will not be discussed in this paper; however, various equations [13, 14] exist that describe an upper limit. These upper limits tend to overestimate the thermal conductivity rather strongly, which made it less useful to include these curves in Fig. 7.

5. SUMMARY

The use of the finite element method to calculate the conductivity of a matrix containing a dispersed phase is shown. The FEM accounts for the influence of the shape, the orientation and the distribution of the dispersed phase material on the conductivity. The

2D conductivity, that is directly obtained from the FEM calculations, is a useful lower limit of the actual 3D conductivity. The thermal conductivity of a matrix containing spherical particles can be used as a upper limit of the overall thermal conductivity in the case that $\lambda_D < \lambda_M$. A simple relation is obtained that transfers the 2D conductivity into the 3D conductivity. The influence of the microstructure of irradiated UO_2 on the conductivity has been computed as an example of the use of the FEM.

Fig. A1. The geometries with the minimum influence of the dispersed phase on the conductivity: (a) the minimum decrease for $\lambda_D < \lambda_M$; (b) the minimum increase for $\lambda_D > \lambda_M$.

REFERENCES

1. MacEwan, J. R., Stoute, R. L. and Notley, M. J. F., Effect of porosity on the thermal conductivity of UO_2. *Journal of Nuclear Materials*, 1967, **24,** 109–112.
2. Goldsmith, L. A. and Douglas, J. A. M., Measurement of the thermal conductivity of uranium dioxide at 670–1270 K. *Journal of Nuclear Materials*, 1973, **47,** 31–42.
3. Agapiou, J. S. and DeVries, M. F., An experimental determination of the thermal conductivity of 304L stainless steel powder metallurgy materials. *ASME Journal of Heat Transfer*, 1989, **111,** 281–286.
4. Maxwell, J. C., *Treatise on Electricity and Magnetism*, Vol. 1. Oxford University Press, Oxford, 1873/1904.
5. Loeb, A. L., Thermal conductivity: VIII, a theory of thermal conductivity of porous materials. *Journal of American Ceramics Society*, 1954, **37,** 96–99.
6. Schulz, B., Die abhängigkeit der Feldeigenschaften zweiphasiger Werkstoffe von ihrem Gefügeaufbau, KFK 1988, Kernforschungszentrum Karlsruhe, Karlsruhe, 1974, Also in Schulz, B., *High Temperature—High Pressure*, 1981, **13,** 649–653.
7. Cunningham, M. E. and Peddicord, K. L., Heat conduction in spheres packed in an infinite regular cubical array. *International Journal of Heat and Mass Transfer*, 1981, **24,** 1081–1088.
8. Tzou, D. Y., The effect of internal heat transfer in cavities on the overall thermal conductivity. *International Journal of Heat and Mass Transfer*, 1991, **34,** 1839–1846.
9. Alvis, J. M., Thomas, J. K. and Peddicord, K. L., Cermet fuel thermal conductivity. *Transactions of the American Nuclear Society*, 1991, **64,** 269–270.
10. Bauer, T. H., A general analytical approach toward the thermal conductivity of porous media. *International Journal of Heat and Mass Transfer*, 1993, **36,** 4181–4191.
11. Bakker, K., Kwast, H. and Cordfunke, E. H. P., The contribution of thermal radiation to the thermal conductivity of porous UO_2. *Journal of Nuclear Materials*, 1995, **223,** 135–142.
12. Landau, L. D. and Lifschitz, E. M., *Electrodynamics of Continuous Media*. Pergamon Press, Oxford, 1975, p. 26.
13. Hashin, Z. and Shtrikman, S., A variational approach to the theory of the effective magnetic permeability of multiphase materials. *Journal of Applied Physics*, 1962, **33,** 3125–3131.
14. DeVera Jr, A. L. and Strieder, W., Upper and lower bounds on the thermal conductivity of a random, two phase material. *Journal of Physics and Chemistry*, 1977, **81,** 1783–1790.

APPENDIX

1.1. *Introduction*

The change of the conductivity due to the dispersed phase can be described as the sum of two parts, both in 2D and in 3D. Part 1 describes the maximum overall conductivity in the case $\lambda_D < \lambda_M$ and the minimum overall conductivity in the case of $\lambda_D > \lambda_M$. These maximum and minimum overall conductivities represent the conductivities that are closest to λ_M for a certain amount of dispersed phase. Part 2 describes the additional decrease of the conductivity for $\lambda_D < \lambda_M$ and the additional increase of the conductivity for $\lambda_D > \lambda_M$ due to the influence of the shape of the dispersed phase. By combining both parts a relation is obtained that transfers the 2D conductivity into the 3D conductivity.

1.2. *Part* 1

The parallel geometry (Fig. A1(a)) induces the minimum decrease of the conductivity in the case of a dispersed phase with $\lambda_D < \lambda_M$. The conductivity (both for 2D and 3D) of this geometry is described by equation (A1).

$$f_{2D} = f_{3D} = \frac{\lambda_D c_D + \lambda_M (1 - c_D)}{\lambda_M} \quad (\lambda_D < \lambda_M) \qquad \text{(A1)}$$

The minimum increase of the conductivity in the case of a dispersed phase with $\lambda_D > \lambda_M$ is described by the series geometry (Fig. A1(b)). The conductivity (both for 2D and 3D) of this geometry is described by equation (A2).

$$f_{2D} = f_{3D} = \frac{\lambda_D \lambda_M}{c_D \lambda_M + \lambda_D - c_D \lambda_D} \quad (\lambda_D > \lambda_M). \qquad \text{(A2)}$$

1.3. *Part* 2

In the previous section the minimum decrease (for $\lambda_D < \lambda_M$) or the minimum increase (for $\lambda_D > \lambda_M$) of the conductivity has been discussed. The actual change of the conductivity (both in 2D and in 3D) is the sum of this minimal change and a second part that depends on the shape of the dispersed phase. The influence of this second part is assumed to be proportional to the amount of dispersed phase material. For $\lambda_D < \lambda_M$ the combined influence of both parts on the overall conductivity can be described as:

$$f_{iD} = \frac{\lambda_D c_D + \lambda_M (1 - c_D)}{\lambda_M} - a_{iD} c_D \quad (\lambda_D < \lambda_M) \quad (i = 2, 3). \qquad \text{(A3)}$$

For $\lambda_D > \lambda_M$ the combined influence of both parts on the overall conductivity can be described as:

$$f_{iD} = \frac{\lambda_D \lambda_M}{c_D \lambda_M + \lambda_D - c_D \lambda_D} + a_{iD} c_D \quad (\lambda_D > \lambda_M) \quad (i = 2, 3). \qquad \text{(A4)}$$

a_{iD} ($i = 2, 3$) are constants that characterize the influence of the shape of the dispersed phase particles on the conductivity in the 2D and the 3D case, respectively. a_{3D} is smaller than, or equal to, a_{2D} for $\lambda_D < \lambda_M$, while a_{3D} is larger than, or equal to, a_{2D} for $\lambda_D > \lambda_M$.

1.4. *Results*

In the previous section equations have been given for the 2D and the 3D conductivity, both for $\lambda_D > \lambda_M$ and for $\lambda_D < \lambda_M$. The 2D and the 3D equations will be combined in order to obtain relations that can be used to transfer the 2D conductivity into the 3D conductivity. Combining equation (A3) for i equals 2 and 3 yields:

$$\frac{1-((1-(\lambda_D/\lambda_M))c_D)-f_{2D}}{1-((1-(\lambda_D/\lambda_M))c_D)-f_{3D}}=\frac{a_{2D}}{a_{3D}} \quad (\lambda_D < \lambda_M). \quad \text{(A5)}$$

Combining equation (A4) for i equals 2 and 3 yields:

$$\frac{f_{3D}-b}{f_{2D}-b}=\frac{a_{3D}}{a_{2D}} \quad (\lambda_D > \lambda_M) \quad \text{(A6)}$$

where

$$b=\frac{\lambda_D\lambda_M}{c_D\lambda_M+\lambda_D-c_D\lambda_D}.$$

a_{2D} divided by a_{3D} is named r. In Section 3.4 is shown that r depends on λ_D/λ_M, while r varies only slightly with the amount of dispersed phase material and with the shape of the dispersed phase particles, both for $\lambda_D > \lambda_M$ and for $\lambda_D < \lambda_M$. When the shape of the dispersed phase particles is such that a_{3D} is large, a_{2D} is also large, and when a_{3D} is small, a_{2D} is also small. Hence, r (a_{2D}/a_{3D}) is nearly independent of the shape of the dispersed phase particles, which makes it possible to obtain the 3D conductivity from the 2D conductivity.